Ceramics International 49 (2023) 39850–39861

Contents lists available at ScienceDirect

Ceramics International

journal homepage: www.elsevier.com/locate/ceramint

Rapid densification and mechanical properties of ultra-high-pressure sintered transition metal carbide ceramics

Zhangyi Huang [a,b,1], Jiaochun Zheng [b,1], Mingyu Su [b], Mao Deng [b], Yang Shi [b], Ruichong Chen [b], Qingyuan Wang [a,b,**], Zhijun Wang [a], Jianqi Qi [c], Rui Li [d], Haomin Wang [a,*]

[a] Institute for Advanced Study, Chengdu University, Chengdu 610106, China
[b] School of Mechanical Engineering, Chengdu University, Chengdu 610106, China
[c] College of Physics, Sichuan University, Chengdu 610064, China
[d] Center for Lunar and Planetary Sciences, Institute of Geochemistry, Chinese Academy of Sciences, Guiyang 550081, China

ARTICLE INFO

Handling Editor: Dr. P. Vincenzini

Keywords:
Transition metal carbide
Ceramic
Ultra-high pressure sintering
Plastic deformation
Mechanical property

ABSTRACT

Densifying transition metal carbide (TMC) ceramics is challenging due to their low diffusion coefficient and strong covalent bonding. Ultra-high-pressure sintering (UHPS) is a promising technique for preparing dense ceramic materials at low temperatures, but it is underutilized in TMC ceramics. Herein, we report the successful employment of UHPS at 1500 °C for 3 min with an auxiliary pressure of 7 GPa, yielding TaC, NbC, TiC, and ZrC ceramics with relative densities of 99.3%, 98.9%, 98.2%, and 96.4%, respectively. We demonstrate that the densification mechanism of the TMC ceramic in this investigation encompasses plastic deformation and high-pressure assisted atomic diffusion. Furthermore, we determine the Vickers hardness and fracture toughness of TaC, NbC, TiC, and ZrC ceramics to be 16.5, 15.9, 24.0, and 17.7 GPa and 2.5, 2.9, 2.8, and 1.8 MPa $m^{1/2}$, respectively. Moreover, with increasing temperature from room temperature to 500 °C, the hardness and elastic modulus of all four TMC ceramics gradually decrease, with the hardness declining by approximately 17–25%.

1. Introduction

TMC ceramics exhibit great potential as high-temperature materials owing to their high melting points, exceptional chemical stability, high thermal conductivity, superior mechanical properties, and remarkable irradiation resistance [1–5]. Their bright application prospects include hypersonic vehicles, cutting tools, nuclear fuel cladding, and inert matrix fuels [6,7]. Common TMC ceramics, such as TaC, NbC, TiC, ZrC, and HfC, possess a rock salt structure and belong to the Fm $\bar{3}$ m space group. However, these ceramics have low diffusion coefficients, strong covalent bonds, and high melting points, which result in challenges during their dense ceramic preparation, such as the requirement of high sintering temperatures, significant grain growth, and inferior mechanical properties [8–11]. For example, Korklan et al. employed the hot pressing (HP) technique to sinter ZrC ceramics at a very high temperature of 2150 °C, resulting in a final relative density of 95.9% [12]. Similarly, Namini et al. utilized spark plasma sintering (SPS) to sinter TiC ceramic at 1900 °C, achieving a relative density of 99.4%, but the average grain size grew to around 7 μm [13]. Cedillos-Barraza et al. prepared TaC ceramic with a relative density of 98.2% using SPS at a temperature exceeding 2100 °C. However, the Vickers hardness was only 13.9 GPa which may be due to grain coarsening [10]. Balko et al. successfully obtained NbC ceramic with a mere porosity of 0.19% (relative density 98%) using SPS, but the preparation temperature was as high as 2200 °C [14]. Hence, the development of more efficient sintering technologies for the production of dense TMC ceramics is of great importance.

During the ceramic sintering process, near-complete densification at relatively lower temperatures can be achieved by applying auxiliary pressure [15]. Generally, the sintering temperature decreases as the applied pressure increases [16]. Presently, the widely adopted HP and SPS techniques for producing TMC ceramics are restricted by the sintering molds, and the auxiliary pressure typically ranges from 10 to 100 MPa, with sintering temperatures generally ≥1800 °C. If the auxiliary pressure is increased to the GPa level, the sintering temperature is expected to significantly decrease. Research has indicated that when the

* Corresponding author.
** Corresponding author. Institute for Advanced Study, Chengdu University, Chengdu 610106, China.
E-mail addresses: wangqy@scu.edu.cn (Q. Wang), wanghaomin@cdu.edu.cn (H. Wang).
[1] Zhangyi Huang and Jiaochun Zheng contributed equally to this work.

https://doi.org/10.1016/j.ceramint.2023.09.152
Received 16 June 2023; Received in revised form 1 September 2023; Accepted 14 September 2023
Available online 21 September 2023

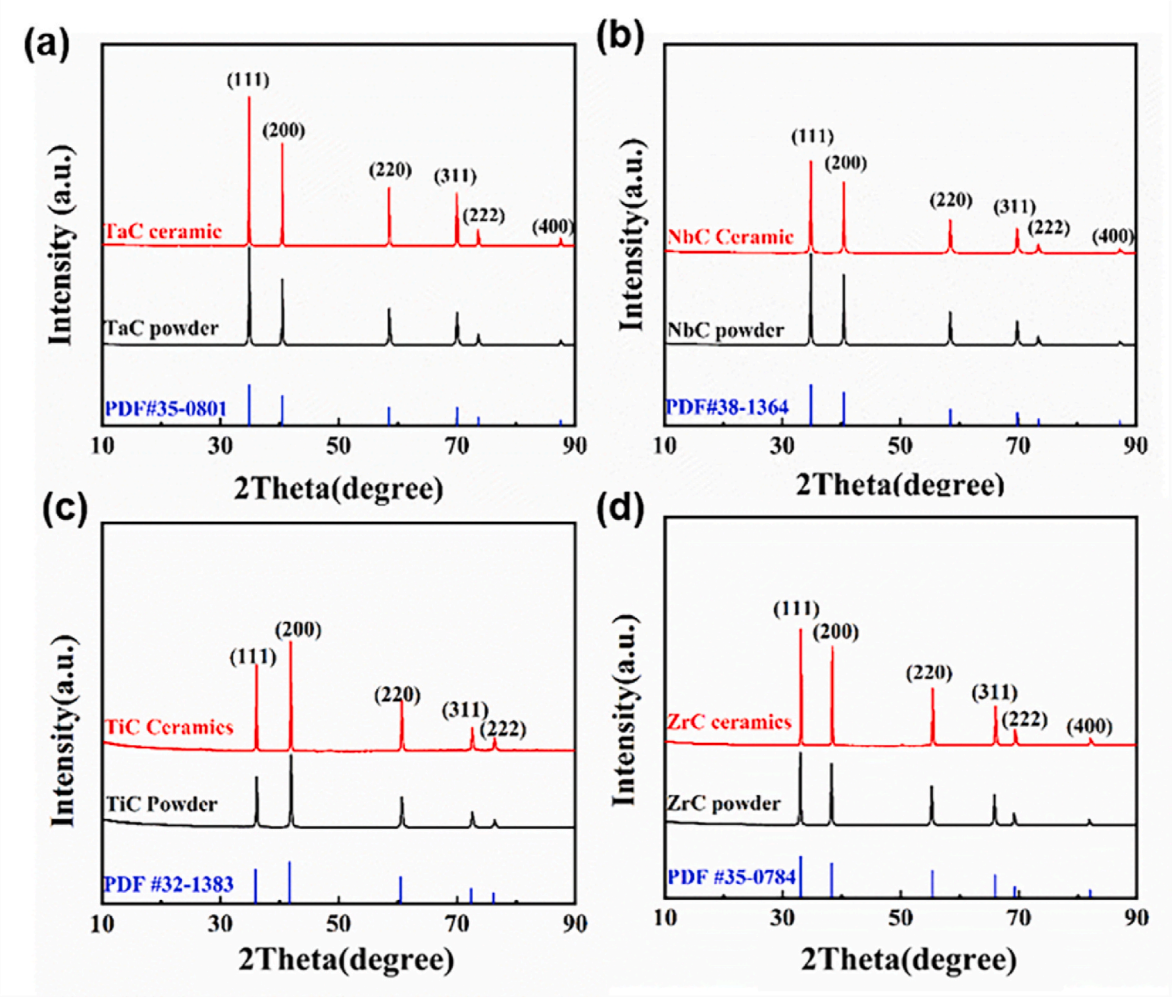

Fig. 1. XRD patterns of TMC powders and ceramics, specifically those of (a) TaC, (b) NbC, (c) TiC, and (d) ZrC.

sintering pressure is 5 GPa, ceramic materials can achieve >99% relative density at sintering temperatures even as low as 0.2 times the melting point of the sintered materials [17,18]. Nonetheless, there is currently limited research on the utilization of UHPS technology for the production of TMC ceramics.

Based on the above issues, this study aims to employ UHPS technology to prepare four common TMC ceramics, namely TaC, NbC, TiC, and ZrC, at a relatively low temperature of 1500 °C with auxiliary pressures in the GPa level. The phases and microstructures of the four TMC ceramics before and after sintering were investigated, and the dominant densification mechanism was analyzed. Moreover, considering the application scenarios of TMC ceramics, we comprehensively compared and analyzed the mechanical properties of the obtained TMC ceramics, including Vickers hardness and fracture toughness, as well as hardness and modulus in the temperature range of 25–500 °C. The research findings may have significant reference value for the future design and preparation of high-performance carbide ceramics.

2. Experimental procedures

2.1. Fabrication of TMC ceramics

The main objective of this work is to prepare dense TMC ceramics. The specific experimental process is outlined as follows. Initially, we acquired four different types of TMC powders, including TaC (99.5%, 3 μm), NbC (99%, 1–4 μm), TiC (99%, 2–4 μm), and ZrC (99%, 1 μm), which were all purchased from Shanghai Aladdin Bio-Chem Technology Co. Ltd. Subsequently, These powders were ball-milled with WC balls of 3 mm in diameter to eliminate powder aggregation. The ball milling conditions consisted of a ball-to-powder ratio of 3:1, ethanol as the ball milling medium, a ball milling speed of 200r/min, and a ball milling time of 6 h, with 5 min of milling followed by 5 min of rest to avoid overheating. Afterward, the powders were dried at 80 °C and passed through a 200-mesh sieve. Next, cold isostatic pressing was employed to granulate the powders at 200 MPa for 15 min to obtain powders with a higher packing density. Then, the granulated powders were filled into a high-pressure assembly for ultra-high-pressure sintering. The specific configuration of the high-pressure assembly involved enclosing the sample with a graphite tube, which acted as a heater. The graphite tube was surrounded by a dolomite tube, which served as an insulating material, and a pyrophyllite cubic cell, which served as a pressure transmission medium. The conditions for ultra-high-pressure sintering were as follows: a holding time of 3 min at 1500 °C, an auxiliary pressure of 7 GPa, and a ramping rate of 200 °C/min. The diameter of the sintered ceramic samples is approximately 13 mm, and the thickness is about 7 mm. Finally, we performed surface grinding and polishing treatment on the sintered ceramic samples until a mirror-like finish was achieved.

2.2. Characterizations

The phase compositions of the TMC powders and ceramics were ascertained via X-ray diffraction (XRD) analysis utilizing monochromatic Cu Kα irradiation (λ = 1.5405 Å) using a Bruker D8 Advance XRD instrument (Bruker Co., Germany). The bulk densities of the

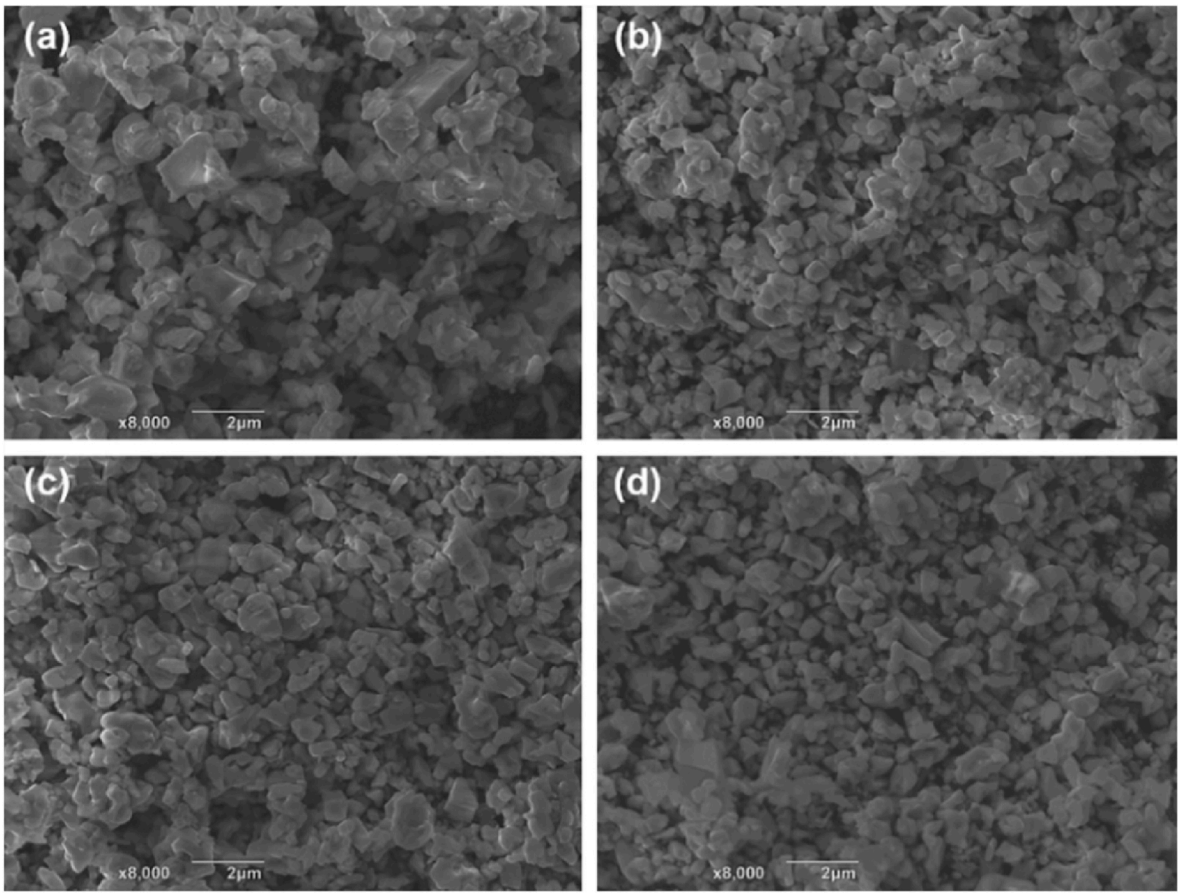

Fig. 2. SEM images of ball-milled (a) TaC, (b) NbC, (c) TiC, and (d) ZrC powders.

ceramics were determined using the Archimedes principle, whereby a density balance and distilled water as an immersion medium were employed. The microstructure of the ball-milled powders was characterized using a field emission scanning electron microscope (FESEM) (JIB-4700, JOEL, Japan). The surface microstructure and grain information (grain size, and grain boundary) were investigated by electron backscatter diffraction analysis (EBSD, Ultim Max, Oxford Instruments, UK) on the FESEM. Before EBSD testing, the ceramic samples underwent sequential grinding with diamond sandpaper and vibrational polishing with diamond paste until the scratches on the surface disappeared and mirror reflection was shown. High-resolution EBSD image was collected on the polished sample with an area of 100 μm × 100 μm using a step size of 0.1 μm. The crystal orientation and geometrically necessary dislocation (GND) density were determined based on the measured EBSD map using the AZtecCrystal software. We use Nano Measure software to statistically count the average grain sizes of the ceramics from inverse pole figures. The mechanical properties of the TMC ceramics were measured using a Nanoindentation Tester (Nanotest Vantage) equipped with a diamond Berkovich indenter produced by Micro Materials. The loading force for the indentation experiments was set to 500 mN, with a loading and unloading rate of 25 mN/s. At least 10 indentations were performed under each condition to ensure accuracy and minimize errors. A high-temperature module equipped with the nanoindentation apparatus was used to investigate the mechanical properties of TMC ceramics at high temperatures. A dual-heating method for both the sample and the indenter was employed. The ceramic sample was glued onto a high-temperature sample stage using a high-temperature adhesive and left to stabilize for 24 h before the experiment. The sample was then mounted onto the nanoindentation tester, and the indenter tip was positioned approximately 300 μm above the sample surface. The sample and indenter were heated to temperatures ranging from 100 to 500 °C at a heating rate of 1.5 °C/min before the in-situ high-temperature indentation experiments were performed at a constant power to prevent temperature fluctuation. The loading force and loading/unloading rate were identical to those used for room temperature indentation experiments. To reduce measurement errors, at least 10 high-temperature indentations were performed at each temperature. The fracture toughness of the ceramic samples was determined using the Vickers indentation crack method [19]. The Vickers indentation is commonly employed to measure the fracture toughness of ceramic materials [19], which can be assessed by the equation below using the length of the indentation crack [20]

$$K_{IC} = 0.016 \bullet \left(\frac{E}{H}\right)^{1/2} \bullet \left(\frac{P}{c^{3/2}}\right) \quad (1)$$

where E is the modulus in GPa, H is the hardness in GPa, P is the indentation load in N, and c is the crack length in m. The sample was indented using a Vickers indenter, and the crack length was measured using SEM image and Image J software. The fracture toughness value was then calculated based on the crack length [21]. Microstructures of the sintered samples were investigated by transmission electron microscopy (TEM, F200, JEOL, Japan). TEM samples were prepared using the standard lift-out method, which involved extracting thin sections from the bulk material using a focused ion beam (FIB, Helios G4 UX, FEI, USA).

3. Results and discussion

3.1. Characterizations of powders and ceramics

Fig. 1 shows the XRD patterns of TMC powders and ceramics. TaC,

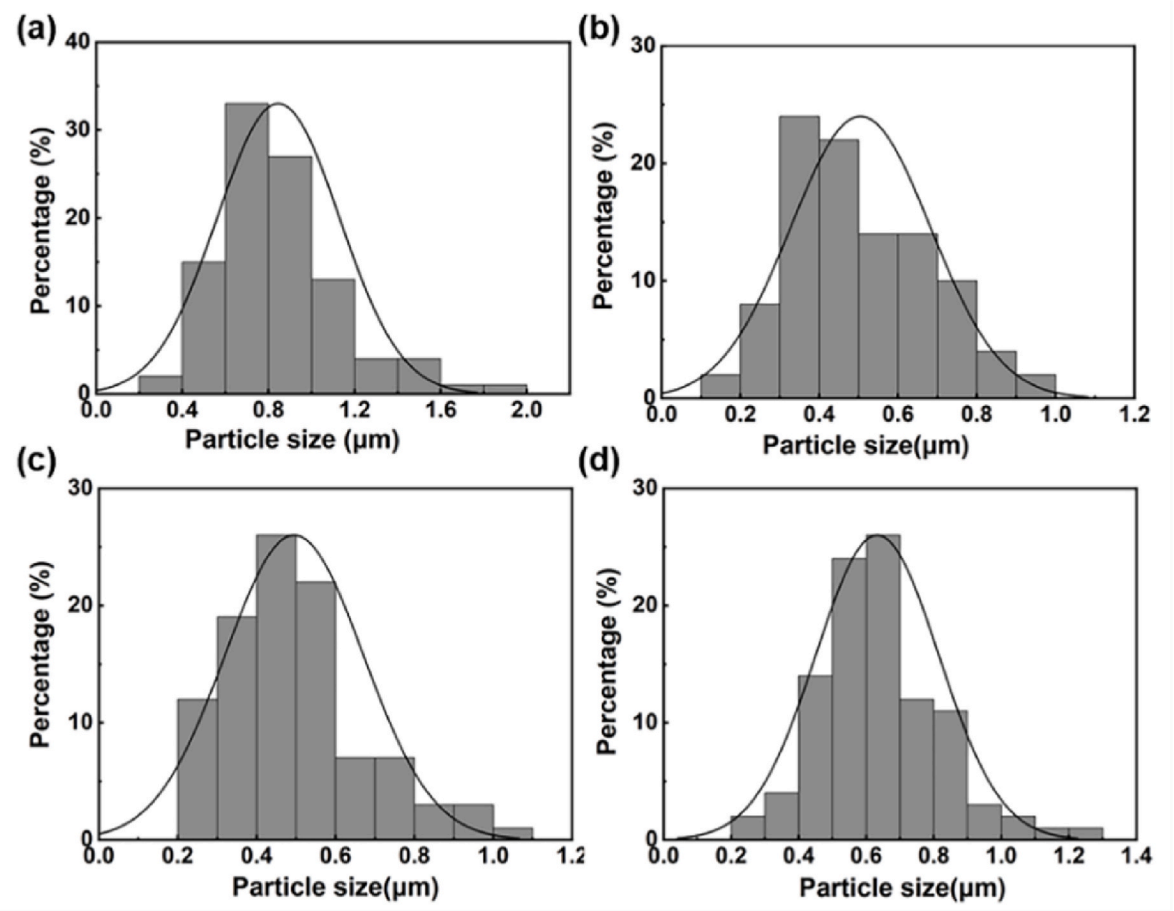

Fig. 3. Particle sizes of ball-milled (a) TaC, (b) NbC, (c) TiC, and (d) ZrC powders.

NbC, TiC, and ZrC are all refractory TMCs that crystallize in the cubic crystal with a rock salt structure. The XRD results confirmed that the four types of TMC powders retained their pure rock salt structure after ultra-high-pressure sintering, without undergoing any phase transitions.

According to the data sheets of raw materials, the particle sizes of the four types of TMC primary powders all fall within the range of 1–4 μm. Fig. 2 illustrates that despite the continued presence of agglomeration after ball milling, a substantial number of monodispersed small particles were formed, indicating that the ball milling process mitigated the degree of agglomeration to a certain extent. An examination of the statistical analysis of the particle size distribution of the powders has shown that the formation of submicron-sized particles reduced the average sizes of ball-milled TaC, NbC, TiC, and ZrC powders to 0.8, 0.5, 0.5, and 0.7 μm, respectively, as illustrated in Fig. 3.

Fig. 4 displays the inverse pole figures of TMC ceramics, which were obtained via the EBSD technique. All four types of TMC ceramics exhibit random crystallographic orientation distribution. The IPF map can be used to measure the grain size of the TMC ceramics. Fig. 5 displays the grain size distributions of four types of TMC ceramics. The average grain sizes of TaC, NbC, TiC, and ZrC ceramics are 1.0 ± 0.6, 2.0 ± 1.1, 1.4 ± 0.8, and 1.1 ± 0.9 μm, respectively, which are lower than the grain sizes of most TMC ceramics. This observation indicates that limited grain growth occurs during the densification process. Fig. 6 presents the surface morphology of polished TMC ceramics. All four types of TMC ceramics exhibit a relatively dense microstructure, but a few small pores are present within the grain interiors and along the grain boundaries. In comparison, ZrC ceramic has the highest number of residual pores within grains. The relative densities of TaC, NbC, TiC, and ZrC, as determined by the density tests, are 99.3%, 98.9%, 98.2%, and 96.4%, respectively, indicating that the densification process of these ceramics reached the final stage according to the theory of ceramic sintering [22]. It is widely known that TMC ceramics exhibit strong covalent bond character and low self-diffusion coefficients, making it difficult to densify them using widely reported sintering techniques, such as HP and SPS [1,23,24]. Table 1 presents some representative results of the sintering conditions and product characteristics of four types of TMC ceramics. It can be observed that in this study, the relative densities of TaC and NbC ceramics sintered at 1500 °C under 7 GPa for 3 min are higher than those prepared by HP or SPS at temperatures greater than 1800 °C, even up to 2300 °C. The density of ZrC ceramics prepared at 1500 °C in our study is quite close to that of ZrC ceramics prepared by other researchers at temperatures greater than or equal to 2000 °C. Therefore, it can be seen that UHPS has unique advantages for the preparation of high melting point TMC ceramics, such as low sintering temperature, short holding time, high degree of densification, and limited grain growth. However, it is worth noting that the relative density of TiC ceramics in this study (98.2%) is slightly lower than that of SPSed at 1600 or 1900 °C, and only slightly higher than that of TiC ceramic prepared by pressureless sintering (PS) at 1700 °C. This may be due to the lower melting point of TiC (3027 °C) compared to TaC (3768 °C), NbC (3600 °C), and ZrC (3427 °C), and the relatively lower temperature required for densification [8]. The abnormal grain growth exhibited by TiC in Fig. 4c may serve as evidence of excessive sintering temperature [25]. Thus, further exploration of the high-pressure sintering temperature conditions in a lower temperature range for TiC may be necessary.

3.2. Densification mechanism

The exceptional capability of TMC ceramics to attain near-theoretical density at a mere 1500 °C can be attributed to the substan-

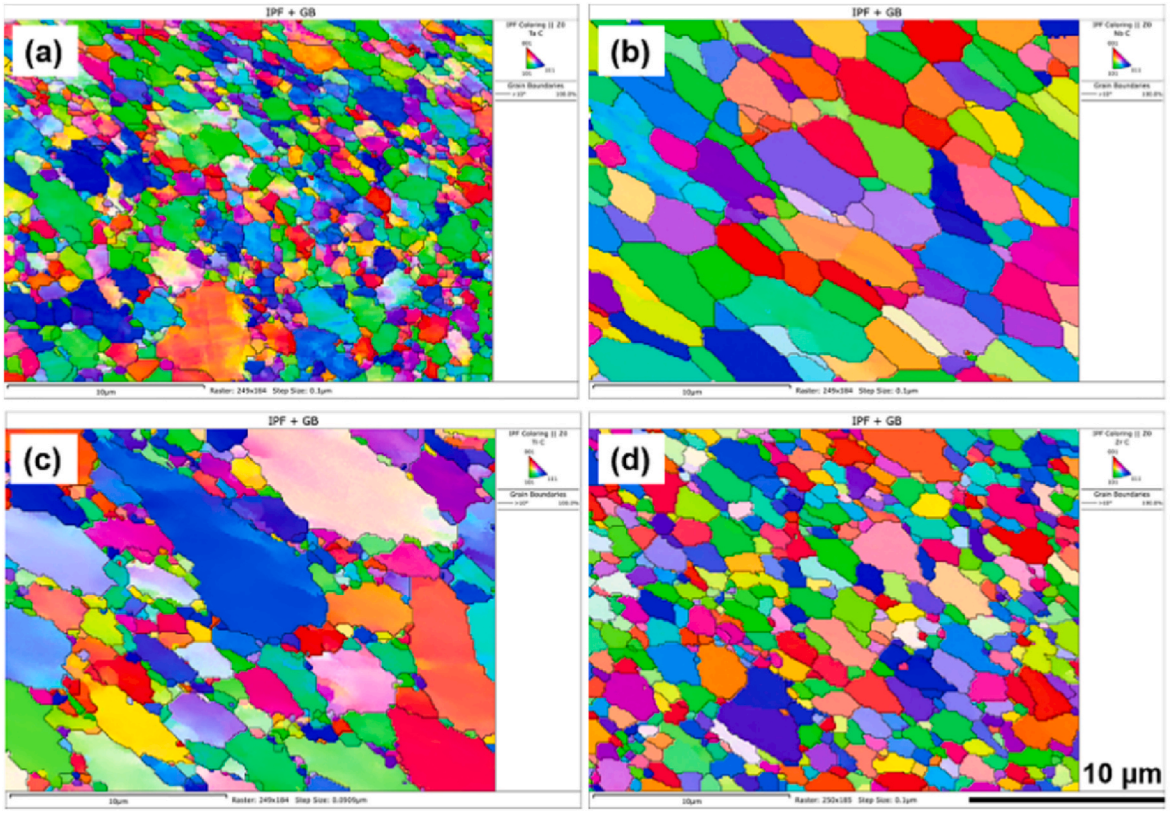

Fig. 4. Inverse pole figures of (a) TaC, (b) NbC, (c) TiC, and (d) ZrC ceramics determined from EBSD analysis.

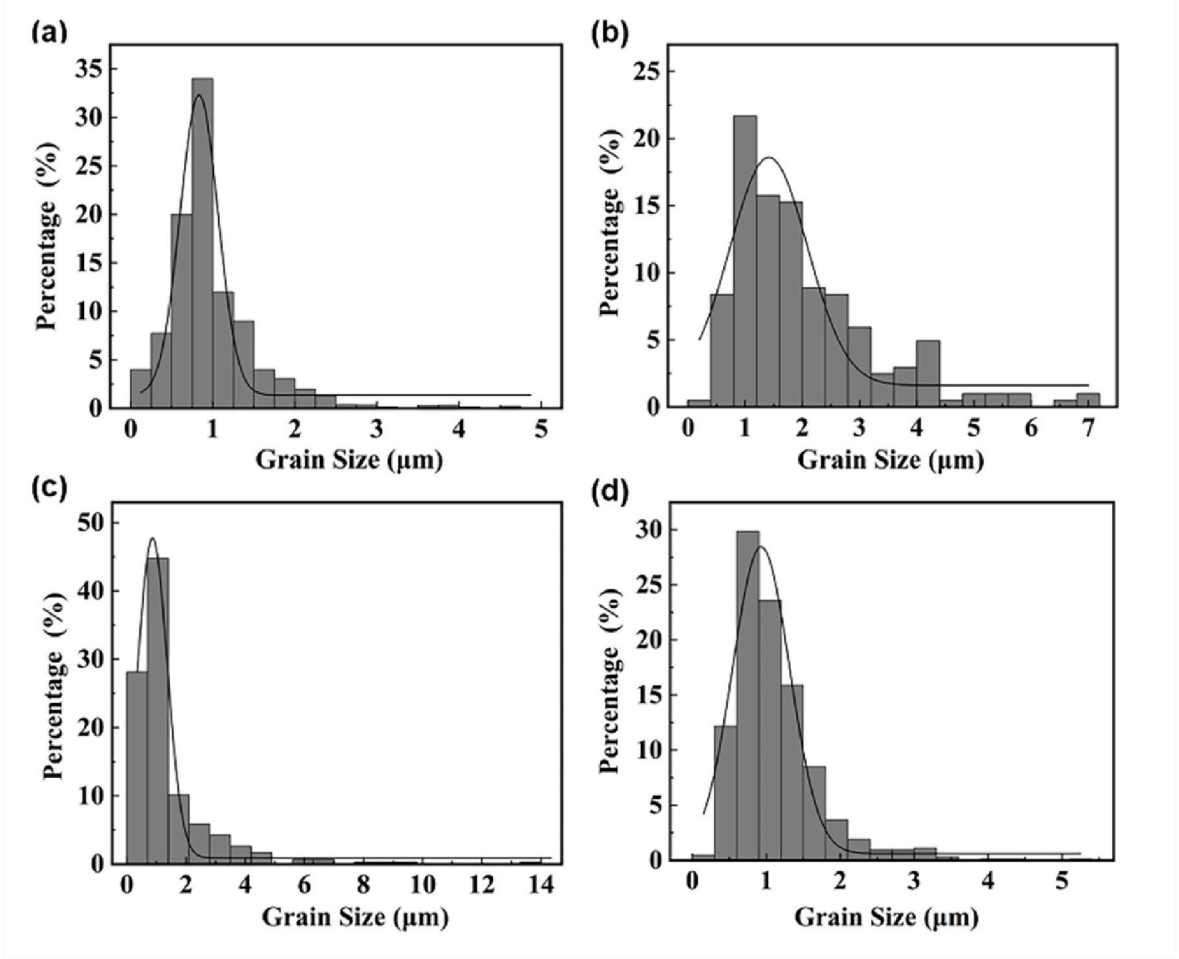

Fig. 5. Grain size distributions of (a) TaC, (b) NbC, (c) TiC, and (d) ZrC ceramics determined from EBSD analysis.

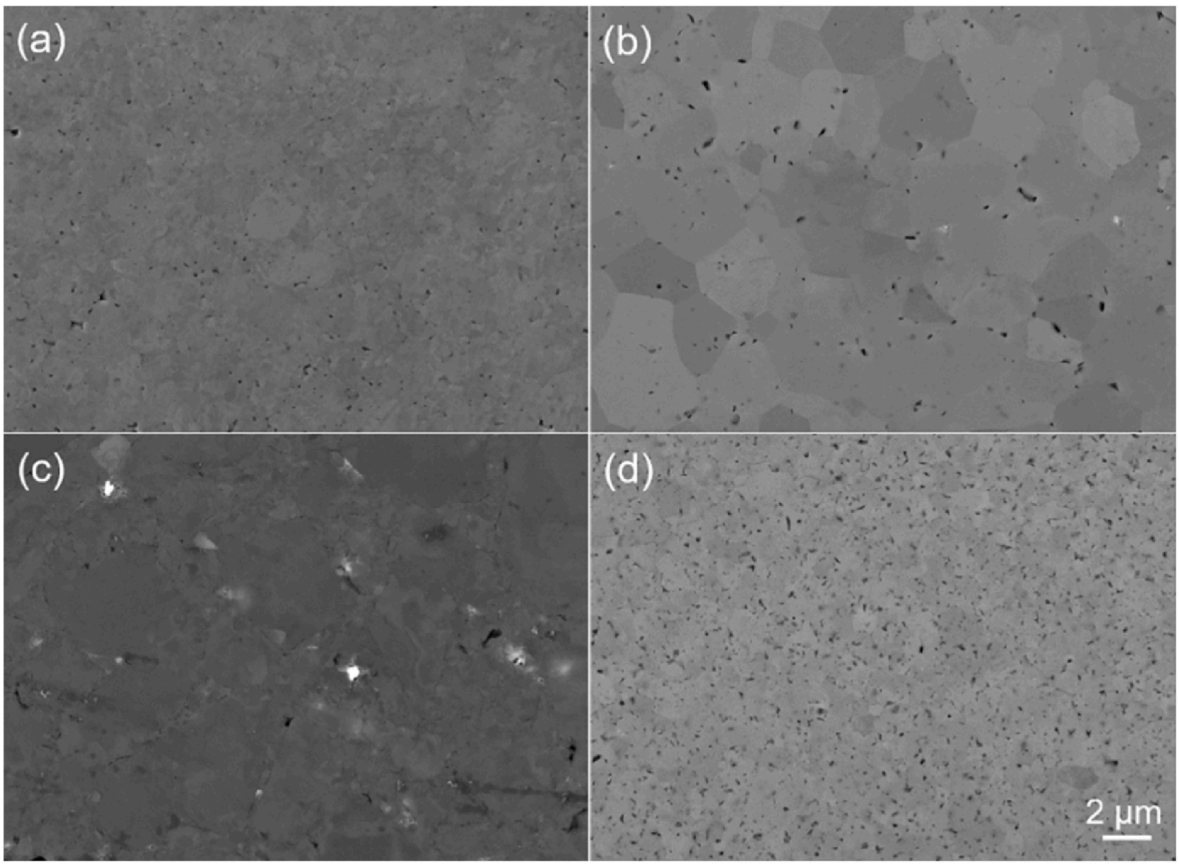

Fig. 6. Microstructures of polished surfaces of (a) TaC, (b) NbC, (c) TiC, and (d) ZrC ceramics.

Table 1
Comparisons of sintering conditions, relative density, grain size, and mechanical properties of TMC ceramics reported in this study and literature.

Mater.	Method	Condition (°C, min, MPa)	R. D. (%)	G. S. (μm)	Hardness (GPa)	Load (N)	F. T. (MPa·m$^{1/2}$)	Ref.
TaC	UHPS	1500, 3, 7000	99.3	1.0	16.5	1.0	2.5	☆
TaC	HP	2300, 45, -	94.3	2.4	14.1	–	3.5	[26]
TaC	SPS	1800, 10, 50	98.5	16	14.3	98	4	[27]
TaC	SPS	1800,10, 80	97.2	2.67	15.6	9.8	3.6	[28]
TaC	HP	1900, 5, 30	85	0.8	11.1	9.8	2.6	[29]
NbC	UHPS	1500, 3, 7000	98.9	2.0	15.9	1.0	2.9	☆
NbC	SPS	1800, 5, 50	99	coarse	18.5	0.98	–	[30]
NbC	HP	2150, 240, 50	98	120	17.3	9.8	–	[31]
NbC	SPS	2200, 30, 35	98	10	17.6	1	3.4	[14]
TiC	UHPS	1500, 3, 7000	98.2	1.4	24.0	1.0	2.8	☆
TiC	SPS	1600, 5, 50	99.9	3.21	30.3	49	4.54	[32]
TiC	SPS	1900, 7, 40	99.4	7	25.7	49	–	[13]
TiC	PS	1700, 60, 0	95.7	5.5	20.3	98	–	[33]
ZrC	UHPS	1500, 3, 7000	96.4	1.1	17.7	1	1.8	☆
ZrC	SPS	2000, 5, 40	94.0	6.5	16.5	9.8	–	[16]
ZrC	HPSPS	2000, 5, 200	97.7	6.4	20.5	9.8	2.65	[16]
ZrC	HP	2150, 35, 32	95.9	2.71	17	–	2.9	[12]
ZrC	SPS	2000, 5, 30	97.8	10.5	18.7	–	2.4	[34]

R. D. is the relative density, G. S. is the grain size, F. T. is the fracture toughness and ☆ represents this work.

tially amplified sintering driving force from an ancillary sintering pressure of 7 GPa. The high-pressure ensemble enveloping the specimen is initially subjected to an external pressure of 7 GPa and subsequently heated. During the former process, stress concentration ensues at the particle contacts as the pressure mounts. The contact stress is reliant on the relative density and is commensurate with the effective pressure (P_E) instead of the externally applied pressure (P_A). Ashby et al. explicate the relationship between P_A and P_E utilizing the ensuing equation [35]:

$$P_E = P_A \bullet \frac{1-\rho_0}{\rho_r^2(\rho_r-\rho_0)} \quad (2)$$

The aforementioned equation explicates the correlation between the relative density of the original green body (ρ_0) and the relative density under elevated pressure (ρ_r). Fig. 7 presents the P_E on the surface of TMC ceramic particles at varying ρ_r. The graphical depiction illuminates that when the ρ_r is low, the P_E can amplify up to 30–40 times the external P_A. Such elevated P_E can initiate plastic deformation at the particle contacts, instigating a progressive increase in the contact area until the P_E subsides below the material's yield strength (σ_Y). During this course, plastic deformation facilitates the prompt densification of the material. The Skorohod model postulated that the σ_Y of a porous material can be

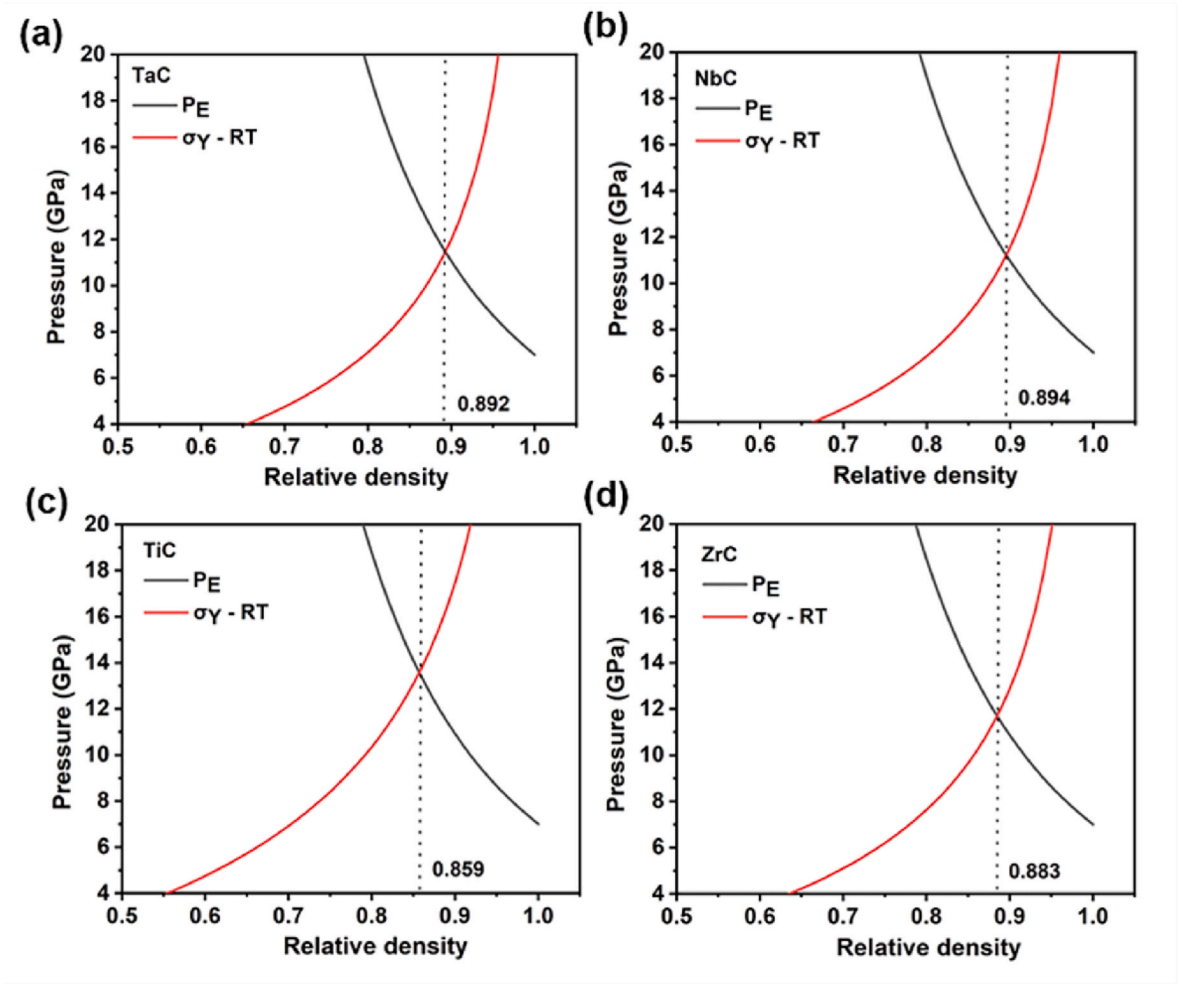

Fig. 7. The effective contact stress (P_E) and the yield stress (σ_Y) of porous (a) TaC, (b) NbC, (c) TiC, and (d) ZrC ceramics, respectively.

articulated as [36]:

$$\sigma_Y = \sigma_0 \sqrt{\frac{2}{3}} \bullet \frac{\rho_r^{3/2}}{(1-\rho_r)^{1/2}} \tag{3}$$

where σ_0 represents the yield strength of fully dense ceramics at ambient temperature. According to Zhang et al.'s findings [37], σ_0 is approximately 0.33 times the material's hardness. Based on this equation, the connection between TMC's σ_Y at ambient temperature and ρ_r is graphed in Fig. 7. It is evident that TaC, NbC, TiC, and ZrC can accomplish nearly 90% relative density at 7 GPa and ambient temperature. Given that the initial relative densities of TMC green bodies are approximately 55%, the plastic deformation experienced under high pressure augments the relative density by more than 30%, thereby constituting the primary mechanism for densification.

Plastic deformation in materials is caused by the motion of dislocations [38,39]. Fig. 8 illustrates the GND distribution obtained through EBSD analysis for the four types of TMC ceramics. It is evident from the illustration that TaC, NbC, TiC, and ZrC ceramics all exhibit substantial internal dislocation densities, measuring 7.7, 4.5, 6.4, and 5.6 × $10^{14}/m^2$ respectively. Ji et al. employed an auxiliary pressure of 200 MPa to sinter ZrC ceramic, consequently observing a high dislocation density within the microstructure of the ceramic [7]. This observation substantiates the prevalence of plastic deformation during the densification process of ZrC ceramics. In comparison, the dislocation density in the TMC ceramics of this study is notably higher. This disparity likely arises from the significantly elevated sintering auxiliary pressure employed in this study, far surpassing 200 MPa, resulting in heightened plastic deformation. Fig. 9 showcases HRTEM images of the TMC ceramics. The illustration reveals the presence of numerous defects within the internal structure of the four TMC ceramics. The IFFT image lucidly depicts the existence of high-density dislocations and stacking faults. These data provide compelling evidence supporting plastic deformation as the predominant mechanism driving densification. As the temperature escalates to 1500 °C, the material's yield strength will diminish due to the thermal softening effect [40,41]. According to Eqs. (2) and (3), the relative density will continue to increase due to enhanced plastic deformation at elevated temperatures. In addition, diffusion-induced densification may be hugely enhanced by the 7 GPa pressure at elevated temperatures due to a large increase in driving force. The ceramic interior, as depicted in Fig. 6, still exhibits enclosed intragranular pores. This strongly indicates that the densification of the TMC ceramic in this study is not solely attributed to plastic deformation under high pressure. Atomic diffusion and high pressure at elevated temperatures can induce creep in the ceramic, resulting in TMC ceramics reaching near-theoretical density [40]. Drawing upon the aforementioned analysis, the densification mechanism of the TMC ceramic in this investigation encompasses plastic deformation and high-pressure assisted atomic diffusion. Notably, plastic deformation emerges as the predominant driver of densification.

3.3. Mechanical properties

Fig. 10 illustrates the Vickers hardness of four TMC ceramics under varying loading forces. Notably, as the load intensifies, the hardness

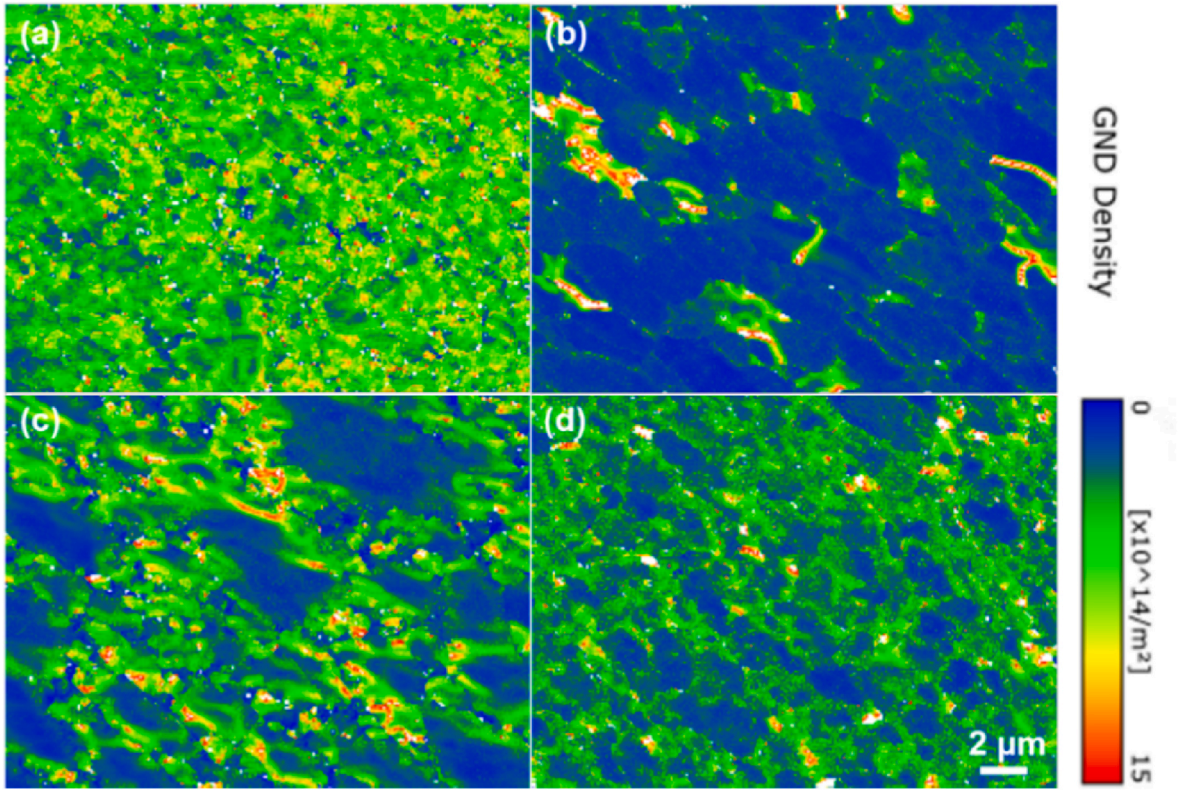

Fig. 8. GND density maps from EBSD results for (a) TaC, (b) NbC, (c) TiC, and (d) ZrC ceramic.

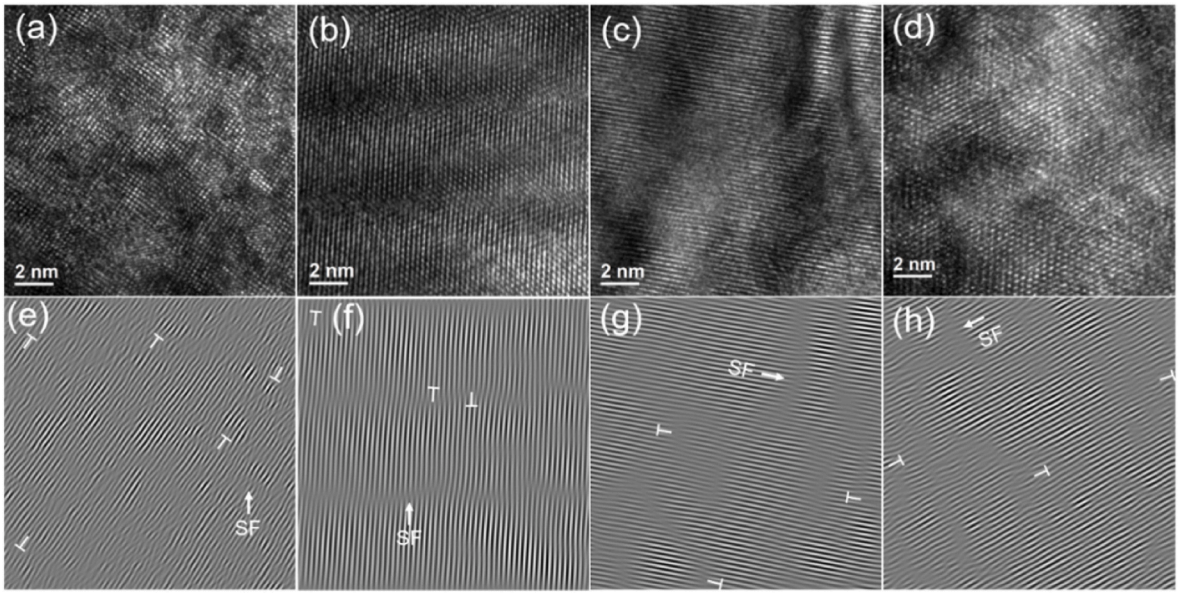

Fig. 9. High-resolution TEM images and corresponding inverse fast Fourier transform (IFFT) images of (a, e) TaC, (b, f) NbC, (c, g) TiC, and (d, h) ZrC ceramic.

gradually diminishes due to the size effect of the indentation, which can be elucidated by the Nix-Gao model [42]. In Table 1, we provide a comparison of the Vickers hardness of TMC ceramics from our study with previous ones. We observed that the Vickers hardness of NbC prepared in our research is slightly inferior to that of the majority of NbC reported in the literature. As for TiC and ZrC, they exhibit average hardness values without any distinct features, whereas our TaC ceramic displays a greater hardness than most others.

Fig. 11 depicts the indentation images of TMC ceramics tested at 0.5 N. As discernible from the figure, cracks conspicuously originate from the vertex of the indentation. We statistically calculated the crack length for each sample and assessed the fracture toughness of the four TMC ceramics. The outcomes reveal that the fracture toughness values of TaC, NbC, TiC, and ZrC are 2.5, 2.9, 2.8, and 1.8 MPa $m^{1/2}$, correspondingly. Notably, ZrC displays the poorest fracture toughness. In comparison with the fracture toughness of other TMC ceramics listed in Table 1 [12–14,30–39], the fracture toughness of TMC ceramics prepared via UHPS still necessitates enhancement.

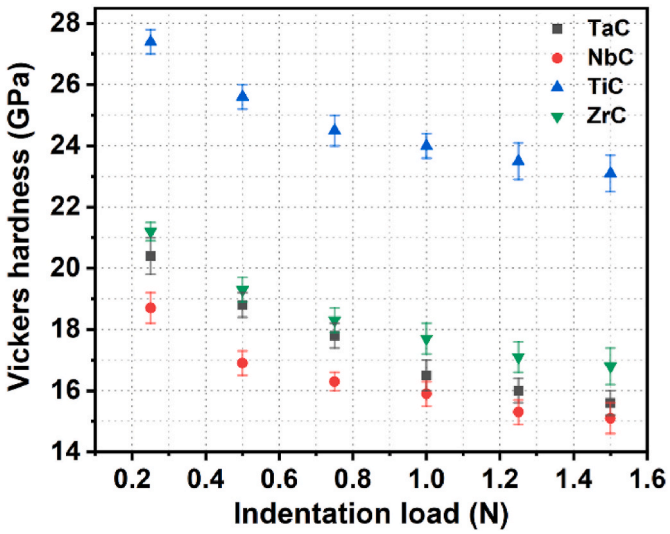

Fig. 10. Vickers hardness of TMC ceramics as a function of indentation load.

In consideration of the utilization of TMC ceramics in high-temperature environments, we have employed nanoindentation to evaluate the hardness and elastic modulus of TMC ceramics within the temperature range of 25–500 °C under a 500 mN load. As illustrated in Fig. 12. The load-displacement curve of TMC ceramic samples at room temperature is continuous and smooth without pop-in. Under a 500 mN load, TaC, NbC, TiC, and ZrC ceramics exhibit maximum depths and contact depths of 1175.4, 1235.8, 1150.5, and 1219.4 nm, as well as 1016.9, 1044.1, 911.0, and 999.9 nm, respectively. It is widely recognized that the deeper the contact depth of material under the same load, the lower its hardness. The microhardness of the four TMC ceramics in order from highest to lowest is TiC (26.2 ± 0.3 GPa) > ZrC (20.2 ± 0.4 GPa) > TaC (19.5 ± 0.3 GPa) > NbC (18.5 ± 0.2 GPa). The elastic modulus can be deduced by analyzing the linear portion of the nanoindentation unloading curve. At room temperature, the elastic modulus of TaC, NbC, TiC, and ZrC ceramics are 401.5 ± 9.2 GPa, 335.8 ± 11.5 GPa, 318.5 ± 15.1 GPa, and 291.6 ± 12.3 GPa, respectively, as demonstrated in Fig. 13. The hardness and elastic modulus of the four TMC ceramics exhibit a monotonic decrease with increasing temperature within the range of 25–500 °C, consistent with the previously reported law [43]. Specifically, the hardness of TaC ceramics declines from 19.5 ± 0.3 GPa at room temperature to 15.1 ± 0.4 GPa at 500 °C, while the elastic modulus decreases from 401.5 ± 9.2 GPa to 291.4 ± 14.2 GPa. The hardness of NbC ceramics also declines from 18.5 ± 0.2 GPa at room temperature to 14.4 ± 0.4 GPa at 500 °C, with the elastic modulus decreasing from 335.8 ± 11.5 GPa to 254.1 ± 13.3 GPa. Similarly, the hardness of TiC ceramics decreases from 26.2 ± 0.3 GPa at room temperature to 21.9 ± 0.2 GPa at 500 °C, while the elastic modulus decreases from 318.5 ± 15.1 GPa to 248.7 ± 13.6 GPa. Lastly, the hardness of ZrC ceramics decreases from 20.2 ± 0.4 GPa at room temperature to 15.2 ± 0.5 GPa at 500 °C, with the elastic modulus decreasing from 291.6 ± 12.3 GPa to 222.9 ± 16.1 GPa. It is worth noting that, despite the decrease in hardness of these four ceramic samples at 500 °C, their values still remain high, with hardness and elastic modulus exceeding 14 GPa and 200 GPa, respectively. The decrease in the elastic modulus of the material at high temperatures is primarily attributed to the weakening of the interaction force between atoms in the material [44]. The relationship between the hardness and yield strength of materials can be described by the reputable Tabor's

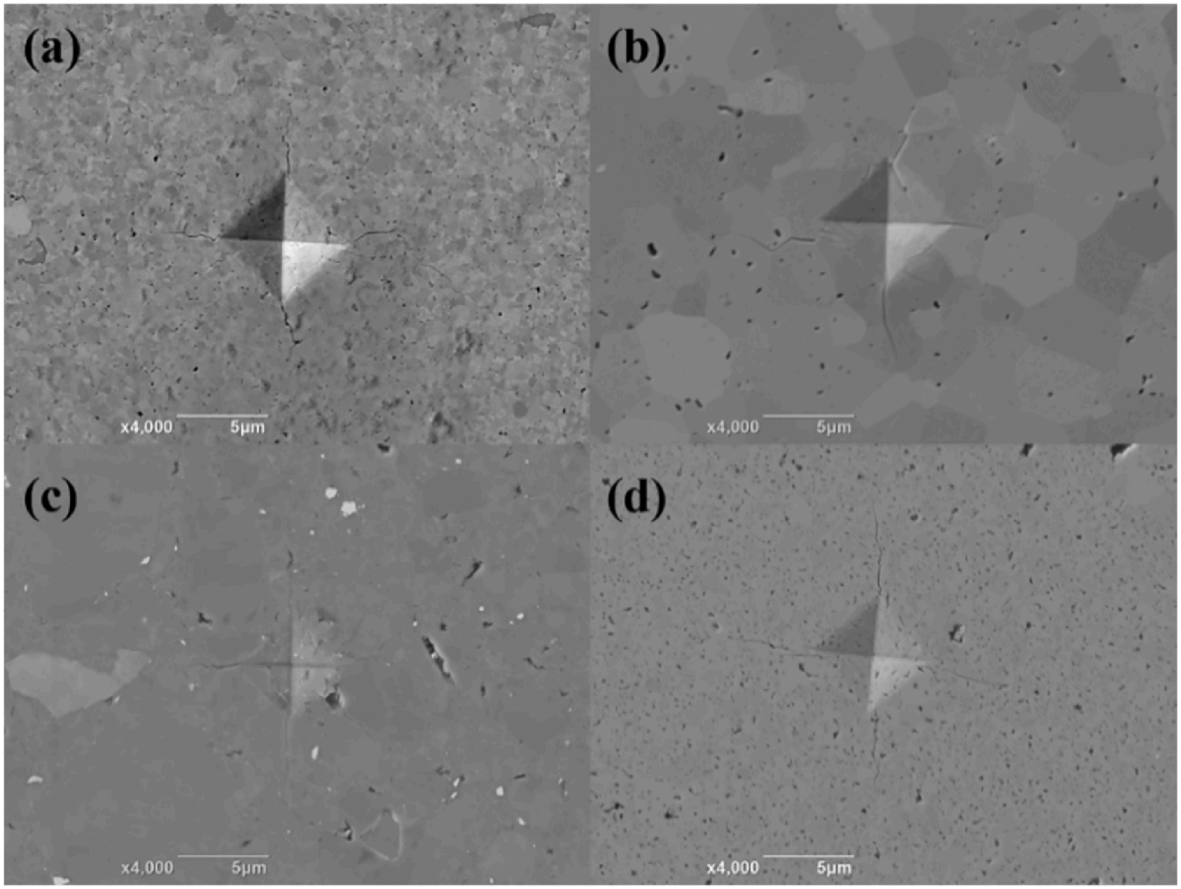

Fig. 11. SEM images of Vickers indentation on TaC, NbC, TiC, and ZrC ceramics at 0.5 N.

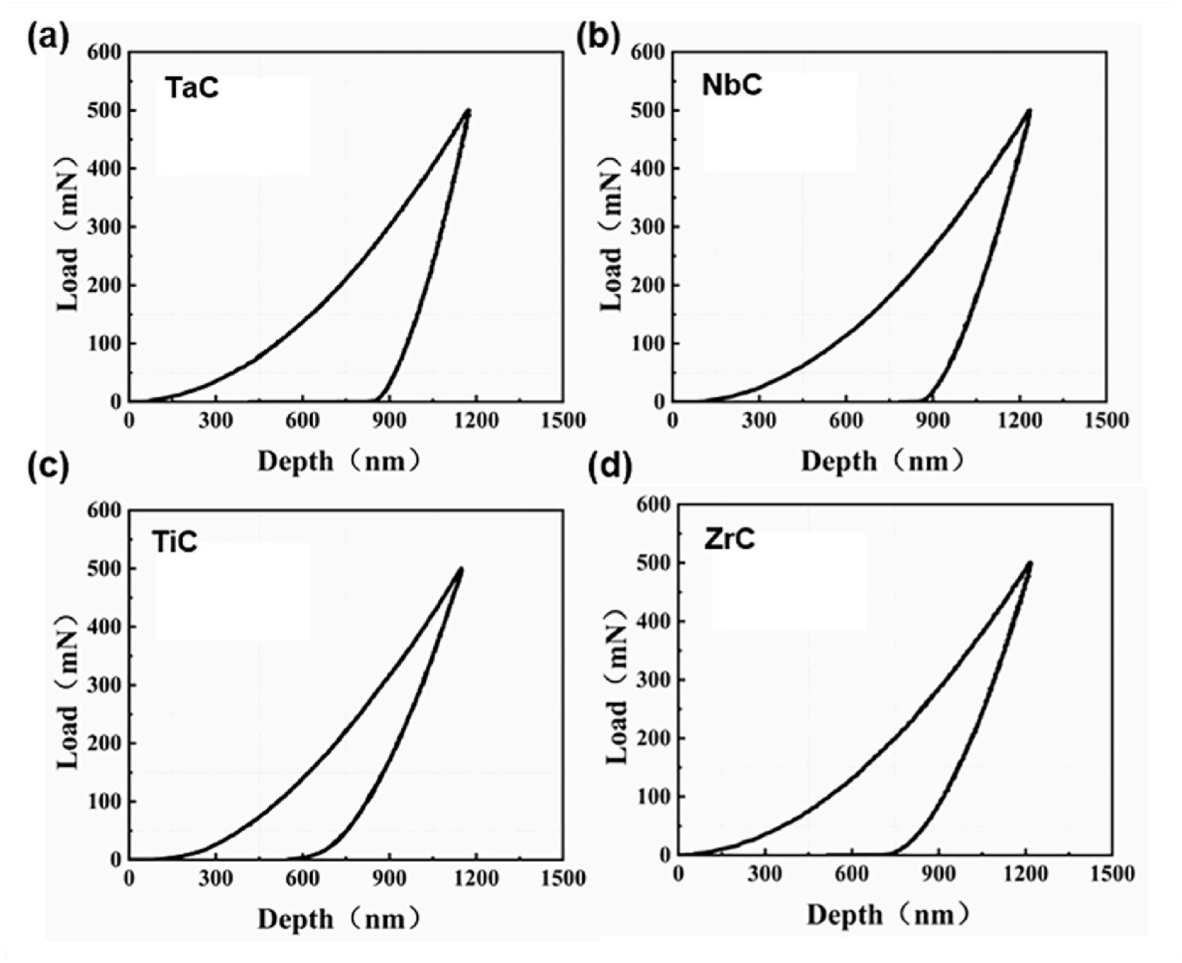

Fig. 12. The load-unload curve of TMC ceramics in 500 mN nanoindentation test.

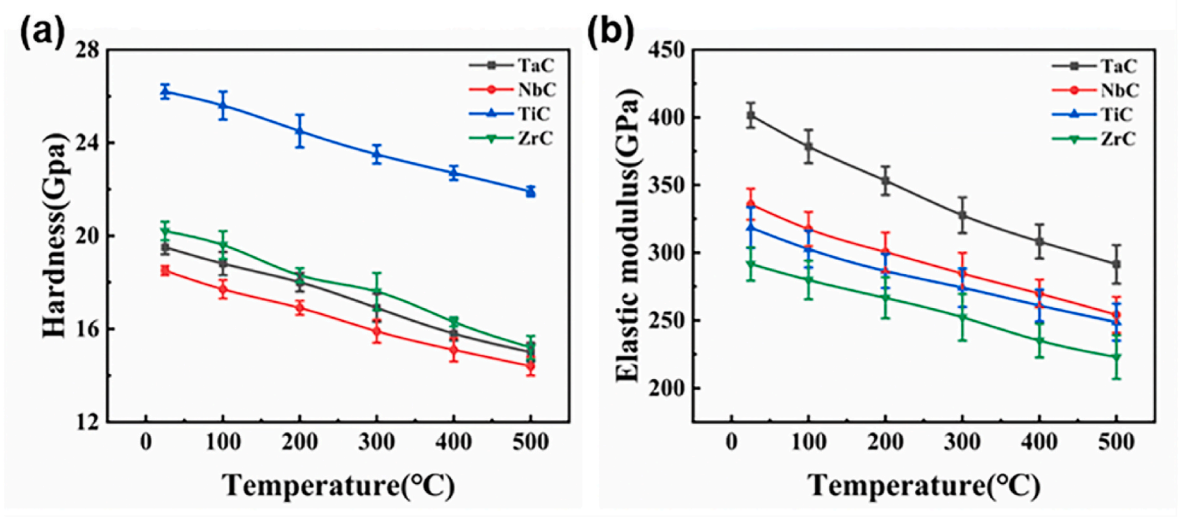

Fig. 13. Nanoindentation (a) hardness and (b) modulus of TMC ceramics at room temperature and elevated temperatures.

rule ($Hv = 3\sigma_0$) [45]. At elevated temperatures, the material's yield strength can be determined by the relationship [36]:

$$\sigma_T = \sigma_0 \bullet \frac{T_m - T}{T_m - T_0} \tag{4}$$

where T_0 is the room temperature and T is the ambient temperature. Thus, the hardness of the four TMC ceramics is expected to theoretically diminish by 13–16% as the temperature escalates from 25 to 500 °C. Nonetheless, in actuality, the decline in hardness is more pronounced, spanning 17%–25%. The modulus reduces 22.0–27.4%. This phenomenon may be attributed to alterations in the surface condition of the

ceramics, such as oxidation reactions. Consequently, we shall undertake more comprehensive research in future studies.

4. Conclusion

In this work, four types of TMC ceramics, including TaC, NbC, TiC, and ZrC, were systematically densified for the first time using the UHPS technology, and their mechanical properties were systematically tested and compared. Specifically, TaC, NbC, TiC, and ZrC ceramics achieve high relative densities of 99.3%, 98.9%, 98.2%, and 96.4%, respectively, after sintering at only 1500 °C for 3 min under an auxiliary pressure of 7 GPa, confirming that the UHPS is an effective technique for the rapid low-temperature preparation of TMC ceramics. We demonstrate that the densification mechanism of the TMC ceramic in this investigation encompasses plastic deformation and high-pressure assisted atomic diffusion. Notably, plastic deformation emerges as the predominant driver of densification. The Vickers hardness and fracture toughness of TaC, NbC, TiC, and ZrC ceramics are 16.5, 15.9, 24.0, and 17.7 GPa and 2.5, 2.9, 2.8, and 1.8 MPa $m^{1/2}$, respectively. Compared with existing research, TaC ceramic exhibits superior mechanical performance, which is attributed to its high relative density of 99.3%. The UHPS process for NbC, TiC, and ZrC needs further exploration to achieve higher relative density and better mechanical performance. The high-temperature nanoindentation results show that as the temperature gradually increases from room temperature to 500 °C, the hardness and elastic modulus of TaC, NbC, TiC, and ZrC decrease linearly, with a hardness reduction of 17%–25% and a modulus reduction of 22.0%–27.4%.

Declaration of competing interest

The authors declare that they have no known competing financial interests or personal relationships that could have appeared to influence the work reported in this paper.

Acknowledgments

This work was supported by the National Natural Science Foundation of China (No. 12205027 and 11802042), the Sichuan Science and Technology Programmer under Grant No. 2022NSFSC1240, and the Foundation of Key Laboratory of Radiation Physics and Technology of the Ministry of Education under Grant No. 2021SCURPT07.

References

[1] W. Zhang, H. Xiang, F.-Z. Dai, B. Zhao, S. Wu, Y. Zhou, Achieving ultra-broadband electromagnetic wave absorption in high-entropy transition metal carbides (HETMCs), J. Adv. Ceram. 11 (4) (2022) 545–555.
[2] B. Ye, T. Wen, M.C. Nguyen, L. Hao, C.-Z. Wang, Y. Chu, First-principles study, fabrication and characterization of $(Zr_{0.25}Nb_{0.25}Ti_{0.25}V_{0.25})C$ high-entropy ceramics, Acta Mater. 170 (2019) 15–23.
[3] R. Florez, M.L. Crespillo, X. He, T.A. White, G. Hilmas, W. Fahrenholtz, J. Graham, The irradiation response of ZrC ceramics under 10 MeV Au^{3+} ion irradiation at 800 °C, J. Eur. Ceram. Soc. 40 (5) (2020) 1791–1800.
[4] Y. Du, J. Gao, X. Lan, Z. Guo, Preparation of TiC ceramics from hot Ti-bearing blast furnace slag: carbothermal reduction, supergravity separation and spark plasma sintering, J. Eur. Ceram. Soc. 42 (5) (2022) 2055–2061.
[5] S.P. Buyakova, E.S. Dedova, D. Wang, Y.A. Mirovoy, A.G. Burlachenko, A. S. Buyakov, Phase evolution during entropic stabilization of ZrC, NbC, HfC, and TiC, Ceram. Int. 48 (8) (2022) 11747–11755.
[6] L. Cheng, Z. Xie, G. Liu, Spark plasma sintering of TiC ceramic with tungsten carbide as a sintering additive, J. Eur. Ceram. Soc. 33 (15–16) (2013) 2971–2977.
[7] B. Ke, W. Ji, J. Zou, W. Wang, Z. Fu, Densification mechanism, microstructure and mechanical properties of ZrC ceramics prepared by high-pressure spark plasma sintering, J. Eur. Ceram. Soc. 43 (8) (2023) 3053–3061.
[8] E. Castle, T. Csanádi, S. Grasso, J. Dusza, M. Reece, Processing and properties of high-entropy ultra-high temperature carbides, Sci. Rep. 8 (1) (2018) 8609.
[9] Y. Pazhouhanfar, A.S. Namini, S.A. Delbari, T.P. Nguyen, Q. Van Le, S. Shaddel, M. Pazhouhanfar, M. Shokouhimehr, M.S. Asl, Microstructural and mechanical characterization of spark plasma sintered TiC ceramics with TiN additive, Ceram. Int. 46 (11) (2020) 18924–18932.
[10] O. Cedillos-Barraza, S. Grasso, N. Al Nasiri, D.D. Jayaseelan, M.J. Reece, W.E. Lee, Sintering behaviour, solid solution formation and characterisation of TaC, HfC and TaC–HfC fabricated by spark plasma sintering, J. Eur. Ceram. Soc. 36 (7) (2016) 1539–1548.
[11] W.S. Williams, Physics of transition metal carbides, Mater. Sci. Eng., A 105 (1988) 1–10.
[12] N. Korklan, G.E. Hilmas, W.G. Fahrenholtz, Processing and room temperature mechanical properties of a zirconium carbide ceramic, J. Am. Ceram. Soc. 104 (1) (2021) 413–418.
[13] A. Babapoor, M.S. Asl, Z. Ahmadi, A.S. Namini, Effects of spark plasma sintering temperature on densification, hardness and thermal conductivity of titanium carbide, Ceram. Int. 44 (12) (2018) 14541–14546.
[14] J. Balko, T. Csanádi, R. Sedlák, M. Vojtko, A. KovalĽíková, K. Koval, P. Wyzga, A. Naughton-Duszová, Nanoindentation and tribology of VC, NbC and ZrC refractory carbides, J. Eur. Ceram. Soc. 37 (14) (2017) 4371–4377.
[15] Z. Huang, Y. Shi, Y. Zhang, M. Deng, Y. Guo, Q. Kong, J. Qi, B. Ma, Q. Wang, H. Wang, An effective strategy for preparing transparent ceramics using nanorod powders based on pressure-assisted particle fracture and rearrangement, J. Adv. Ceram. 11 (12) (2022) 1976–1987.
[16] B. Ke, W. Ji, J. Zou, W. Wang, Z. Fu, Densification mechanism, microstructure and mechanical properties of ZrC ceramics prepared by high-pressure spark plasma sintering, J. Eur. Ceram. Soc. 43 (2023) 3053–3061.
[17] Z. Huang, J. Deng, H. Wang, Y. Zhang, J. Duan, Z. Tang, Z. Cao, J. Qi, D. He, T. Lu, Fast low-temperature densification of translucent bulk nanograin $Gd_2Zr_2O_7$ ceramics with average grain size below 10 nm, J. Alloys Compd. 830 (2020), 154617.
[18] Z. Huang, J. Deng, H. Wang, Y. Zhang, J. Duan, Z. Tang, Y. Yang, D. He, J. Qi, T. Lu, A new method for the preparation of transparent Y2O3 nanocrystalline ceramic with an average grain size of 20 nm, Scr. Mater. 182 (2020) 57–61.
[19] A. Kumar, A. Gokhale, S. Ghosh, S. Aravindan, Effect of nano-sized sintering additives on microstructure and mechanical properties of Si3N4 ceramics, Mater. Sci. Eng., A 750 (2019) 132–140.
[20] J. Lankford, Indentation microfracture in the Palmqvist crack regime: implications for fracture toughness evaluation by the indentation method, J. Mater. Sci. Lett. 1 (11) (1982) 493–495.
[21] K. Song, Y. Xu, N. Zhao, L. Zhong, Z. Shang, L. Shen, J. Wang, Evaluation of fracture toughness of tantalum carbide ceramic layer: a Vickers indentation method, J. Mater. Eng. Perform. 25 (2016) 3057–3064.
[22] M.N. Rahaman, Ceramic Processing and Sintering, CRC press, 2017.
[23] J. Pötschke, M. Dahal, M. Herrmann, A. Vornberger, B. Matthey, A. Michaelis, Preparation of high-entropy carbides by different sintering techniques, J. Mater. Sci. 56 (2021) 11237–11247.
[24] O. Guillon, J. Gonzalez-Julian, B. Dargatz, T. Kessel, G. Schierning, J. Räthel, M. Herrmann, Field-assisted sintering technology/spark plasma sintering: mechanisms, materials, and technology developments, Adv. Eng. Mater. 16 (7) (2014) 830–849.
[25] M. Zhang, Z. Zhou, T. Yuan, R. Li, W. Zhang, Y. Zhang, M. Wang, S. Xie, Analysis of abnormal grain growth behavior during hot-press sintering of boron carbide, Ceram. Int. 46 (10) (2020) 16345–16353.
[26] X. Zhang, G.E. Hilmas, W.G. Fahrenholtz, Densification and mechanical properties of TaC-based ceramics, Mater. Sci. Eng., A 501 (1–2) (2009) 37–43.
[27] A. Nino, T. Hirabara, S. Sugiyama, H. Taimatsu, Preparation and characterization of tantalum carbide (TaC) ceramics, Int. J. Refract. Met. Hard Mater. 52 (2015) 203–208.
[28] C. Liu, A. Wang, T. Tian, L. Hu, W. Guo, Q. He, J. Xie, W. Wang, H. Wang, Z. Fu, Sintering and densification mechanisms of tantalum carbide ceramics, J. Eur. Ceram. Soc. 41 (15) (2021) 7469–7477.
[29] L. Silvestroni, A. Bellosi, C. Melandri, D. Sciti, J. Liu, G. Zhang, Microstructure and properties of HfC and TaC-based ceramics obtained by ultrafine powder, J. Eur. Ceram. Soc. 31 (4) (2011) 619–627.
[30] A. Nino, A. Tanaka, S. Sugiyama, H. Taimatsu, Indentation size effect for the hardness of refractory carbides, Mater. Trans. 51 (9) (2010) 1621–1626.
[31] M. Woydt, H. Mohrbacher, Friction and wear of binder-less niobium carbide, Wear 306 (1–2) (2013) 126–130.
[32] L. Cheng, Z. Xie, G. Liu, W. Liu, W. Xue, Densification and mechanical properties of TiC by SPS-effects of holding time, sintering temperature and pressure condition, J. Eur. Ceram. Soc. 32 (12) (2012) 3399–3406.
[33] Y. Gu, J.-X. Liu, F. Xu, G.-J. Zhang, Pressureless sintering of titanium carbide doped with boron or boron carbide, J. Eur. Ceram. Soc. 37 (2) (2017) 539–547.
[34] X.-F. Wei, J.-X. Song, J.-X. Liu, Y. Qin, F. Li, Y. Liang, G.-J. Zhang, Graphite nanoplatelets toughened zirconium carbide ceramics prepared by spark plasma sintering, Ceram. Int. 47 (6) (2021) 8461–8467.
[35] A. Helle, K.E. Easterling, M. Ashby, Hot-isostatic pressing diagrams: new developments, Acta Metall. 33 (12) (1985) 2163–2174.
[36] M. Meyers, E. Olevsky, J. Ma, M. Jamet, Combustion synthesis/densification of an Al_2O_3–TiB_2 composite, Mater. Sci. Eng., A 311 (1–2) (2001) 83–99.
[37] P. Zhang, S. Li, Z. Zhang, General relationship between strength and hardness, Mater. Sci. Eng., A 529 (2011) 62–73.
[38] N. Fleck, M. Ashby, J. Hutchinson, The role of geometrically necessary dislocations in giving material strengthening, Scr. Mater. 48 (2) (2003) 179–183.
[39] Q. Feng, S. Whang, Deformation of Ti–56 At.% Al single crystals oriented for single slip by 1/2< 110] ordinary dislocations, Acta Mater. 48 (17) (2000) 4307–4321.
[40] R. German, Sintering: from Empirical Observations to Scientific Principles, Butterworth-Heinemann, 2014.
[41] C. Herring, W. Kingston, The Physics of Powder Metallurgy, WE Kingston, Edition, McGraw Hill, New York, 1951.
[42] W.D. Nix, H. Gao, Indentation size effects in crystalline materials: a law for strain gradient plasticity, J. Mech. Phys. Solid. 46 (3) (1998) 411–425.

[43] M. Burtscher, M. Zhao, J. Kappacher, A. Leitner, M. Wurmshuber, M. Pfeifenberger, V. Maier-Kiener, D. Kiener, High-temperature nanoindentation of an advanced nano-crystalline W/Cu composite, Nanomaterials 11 (11) (2021) 2951.

[44] T.-H. Fang, C.-I. Weng, J.-G. Chang, Molecular dynamics analysis of temperature effects on nanoindentation measurement, Mater. Sci. Eng., A 357 (1–2) (2003) 7–12.

[45] D. Tabor, The Hardness of Metals, Oxford University press, 2000.